Journal of Geomine (2024), 2(2), 58-68
DOI: 10.22077/jgm.2025.8356.1038

Seismic analysis of sediments in the Tabriz plain using metaheuristic algorithms and shear wave velocity modeling

Ramin Vafaei Poursorkhabi[1], Shahram Angardi[2], Ahmad Zarean[3]

Recived: 2024 Oct. 27, Revised: 2025 Mar. 07, Online Published: 2025 Mar. 26

ABSTRACT

Surface waves are a cornerstone of geophysical studies for deriving shear wave velocity profiles. Inverting dispersion curves, however, poses a significant challenge for traditional local search methods due to the problem's nonlinearity and the objective function's multiple extrema. This study introduces a metaheuristic approach Ant Colony Optimization (ACO) implemented in MATLAB to tackle these complexities. The algorithm's effectiveness was assessed using synthetic datasets, testing three distinct six-layer models with varying shear wave velocities, compressional wave velocities, and layer thicknesses, assuming a variable Poisson's ratio and constant density. Compared to the neighborhood algorithm in Geopsy software, ACO exhibited superior reliability and computational efficiency. The method was further validated using an experimental dispersion curve from the Tabriz Plain, yielding results closely aligned with borehole data. Subsequently, a two-dimensional shear wave velocity model was constructed for the study area based on these inversion outcomes. This work underscores the promise of metaheuristic optimization techniques in enhancing the accuracy and robustness of surface wave dispersion curve inversion.

KEYWORDS

Metaheuristic optimization, neighborhood algorithm, surface waves, dispersion curve inversion

I. INTRODUCTION

Shear wave velocity (V_S) is a key parameter for evaluating site effects in alluvial sediments, where soft layers overlying stiff bedrock amplify seismic waves during earthquakes (Renalier et al., 2010; Cruz et al., 2024). Accurate V_S profiles are essential for seismic hazard analysis, as they govern site-specific dynamic responses and influence potential structural damage (Somerville & Graves, 2003). Although borehole measurements yield direct V_S data, their high cost and limited spatial coverage restrict their practicality. Surface wave methods, which exploit dispersion curves, provide a non-invasive, cost-effective alternative for V_S profiling in alluvial settings (Zarean et al., 2015; Pourmirzaee, 2016; Maghami et al., 2021; Angardi et al., 2024). These techniques encompass three primary stages: field data acquisition, processing to generate experimental dispersion curves, and inversion to estimate subsurface parameters (Farrugia et al., 2016).

In alluvial environments like the Tabriz Plain, inverting dispersion curves is challenging due to complex layering and sharp velocity contrasts. Traditional local search algorithms often fail to address the nonlinearity and local minima inherent in such inversions (Socco et al., 2010). Consequently, global optimization methods—such as genetic algorithms (Yamanaka & Ishida, 1996), simulated annealing (Beaty et al., 2002), and neighborhood algorithms (Wathelet et al., 2004)—have gained prominence. This study introduces Ant Colony Optimization (ACO), a metaheuristic algorithm, to enhance dispersion curve inversion in alluvial sediments. Its performance is evaluated using synthetic models and field data from the Tabriz Plain.

II. METHODOLOGY

A. *Data Collection*

The field data were acquired using **Geometrics Geode Seismograph** equipped with 40 Hz vertical geophones** arranged in a linear array.

The data were recorded with a sampling rate of 1 ms, using 24 active channels.

A 5 kg sledgehammer with an aluminum strike plate was used as the seismic source.

The receiver spacing was 2 meters, and the total length of the spread was 46 meters.

The measurements were conducted on a dry, level surface to minimize external noise effects.

[1] Islamic Azad University, Tabriz Branch, Tabriz, Iran, [2] Department of Civil Engineering, Islamic Azad University, Tabriz Branch, Tabriz, Iran,
[3] Department of Civil Engineering, Islamic Azad University, Shabestar Branch, Shabestar, Iran
✉ R. Vafaei Poursorkhabi: raminvafaei@yahoo.com

B. Ant Colony Optimization Algorithm

Proposed by Dorigo et al. (1996), ACO emulates the foraging behavior of ants, employing artificial agents that collaborate through pheromone trails to solve optimization problems. In this study, ACO is adapted to invert surface wave dispersion curves by iteratively exploring the parameter space. Each artificial ant constructs a candidate V_S profile guided by pheromone intensity and heuristic information, with transition probabilities governed by Eq.s (1)–(3) (Li et al., 2009). Pheromone evaporation, controlled by the parameter ρ, and deposition regulate the balance between exploration and convergence, enabling the algorithm to adapt to complex alluvial stratigraphy (Duan & Yu, 2007; Zareh et al., 2023). The ACO workflow tailored for this application is depicted in Fig. 3. A key advantage of metaheuristic algorithms like ACO is their flexibility. Unlike deterministic methods, ACO can dynamically adjust to changing conditions without restarting the optimization process. For instance, if an obstacle disrupts the ants' path (Fig. 1a), they explore alternative routes using pheromone-based feedback, rapidly identifying an optimal solution. Upon removal of the obstacle (Fig. 1b), the ants efficiently revert to the original path, leveraging accumulated pheromone information. In this implementation, m artificial ants operate in parallel, each initiating from a randomly selected point i (Fig. 2). The probability of an ant k at point i selecting a subsequent point j is initially uniform due to equal pheromone levels across all paths. As iterations progress, pheromone evaporation and deposition adjust path selection probabilities based on solution quality and heuristic guidance (Li et al., 2009), as expressed in Eq. (1).

$$P_{ij}^{k}(t) = \frac{\tau_{ij}^{\alpha} * \eta_{ij}^{\beta}(t)}{\sum_{l} \tau_{il}^{\alpha} * \eta_{il}^{\beta}(t)}, l, j \in others_{k} \quad (1)$$

In the above formula, the coefficient α represents the influence of pheromone, while β represents the influence of metaheuristic information. These two coefficients establish a balance between metaheuristic information and the amount of pheromone. If we assume α=0, Eq. (1) gets transformed into Eq. (2), and the probability of selection will depend solely on metaheuristic information. As β increases, the probability of selection increases, as well.

$$P_{ij}^{k}(t) = \frac{\eta_{ij}^{\beta}(t)}{\sum_{l} \eta_{il}^{\beta}(t)} \quad (2)$$

If we assume β=0, Eq. (1) transforms into Eq. (3), and the probability of selection will depend solely on the pheromone. As α increases, the probability of selection also increases. The dependence of the selection probability on the amount of pheromone leads to rapid convergence and degradation of the algorithm's solutions.

$$P_{ij}^{k}(t) = \frac{\tau_{ij}^{\alpha}(t)}{\sum_{l} \tau_{il}^{\alpha}(t)} \quad (3)$$

(a)

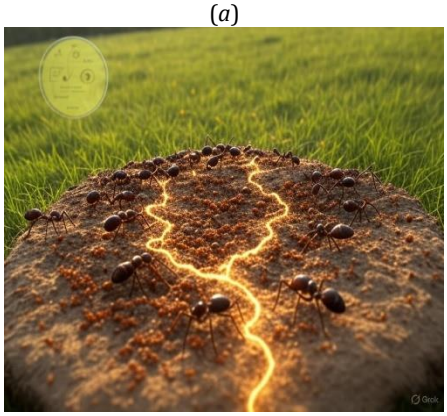

(b)

Fig. 1. (a) Placing an obstacle in the path of ants from the colony to the food source. (b) Removing the obstacle and the flexibility of ant behavior (Dorigo et al., 1996).

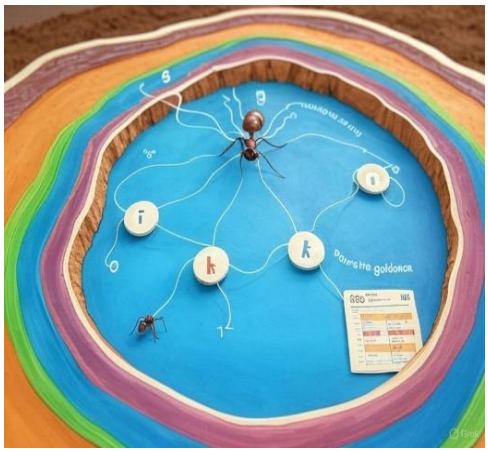

Fig. 2. Path selection by the ant at point i (Li et al., 2009)

To ensure the Ant Colony Optimization (ACO) algorithm identifies the shortest path between the nest and food source, a sufficiently large number of searching ants is essential. This increases the likelihood that all possible routes are explored, facilitating the selection of the optimal path. An insufficient number of ants may lead to two critical issues. First, if an ant independently discovers the food source, the pheromone trail it deposits may evaporate before other ants can follow, rendering the route ineffective. Second, with a limited number of ants, only a subset of paths is evaluated; if the

initial ants select a suboptimal route, the lack of additional exploration may prevent correction, failing to identify the optimal path. Consequently, the number of searching ants must exceed a minimum threshold to guarantee convergence to the optimal solution. Upon completing their paths, each ant's route is evaluated using a fitness function. Subsequently, the fitness of each path is assessed, and the most promising routes are selected as candidate solutions for pheromone deposition. Pheromone updating typically involves two steps. In the first step, pheromones on all edges or nodes evaporate, with the evaporation rate governed by the parameter ρ. A low evaporation rate preserves the influence of successful paths from previous iterations, potentially slowing convergence, whereas a high evaporation rate accelerates convergence by rapidly diminishing outdated trails. In the second step, pheromone secretion is applied, typically restricted to the best-performing ant(s) or a subset of top solutions, as reported in most implementations (Nemati & Basiri, 2011).

$$\tau_{ij}(t+1) = (1-\rho) * \tau_{ij}(t) + \sum \Delta\tau_{ij} \quad (4)$$

$$\Delta\tau_{ij} = \begin{cases} Q & for\ edges\ of\ best\ ant \\ 0 & otherwise \end{cases} \quad (5)$$

Pheromones are secreted in excess; it will highlight the path of the selected ant. It should be noted that initially, the initial amount of pheromone is considered as a percentage between the values (0,1), meaning that it should be in the range (0.001 < pheromone of each element < 1). If the initial pheromone is set to be 0, ultimately, after updating the pheromone, most ants' paths will have a value of 0, and the path corresponding to the best ant will have a value of 1. Consequently, all ants in subsequent iterations will almost exclusively choose the path of the best randomly chosen ant and converge on a path that may not be optimal. Paths that have a pheromone value of 0 will be eliminated from the search process, thus limiting the search space to a few initial random solutions, which are not thoroughly explored. Therefore, it is better to select the initial pheromone value to be something in the range (0,1), specifically around 0.5. Pheromone updating provides indirect positive and negative feedback within the colony. Fig. 3 shows the flowchart of the ant colony algorithm.

III. Application of the Ant Colony Optimization Algorithm for Surface Wave Analysis

This section details the application of the inversion algorithm to synthetic data derived from a direct model, alongside the validation of results against these synthetic datasets. Synthetic response curves for a hypothetical soil model are generated using a direct program and compared with the initial model following inversion. The direct problem in this study is based on the transfer matrix method (Haskell, 1953), which was updated by Herrmann and Ammon (2004) and implemented as Fortran software (Pouraziz et al., 2024). This software was executed within the MATLAB environment to produce synthetic response curves. For each iteration, the synthetic response curve is computed using random parameters from the Ant Colony Optimization (ACO) algorithm, with the misfit value assessed according to Eq. (6). In cases where data uncertainty is present, the misfit function is defined as described by Rui et al. (2022) and Wathelet et al. (2004).

$$misfit = \sqrt{\sum_{i=0}^{n_F} \frac{(x_{di}-x_{ci})^2}{\sigma_i^2 n_f}} \quad (6)$$

A. Inversion of Synthetic Data

In this section, a hypothetical six-layer model is used to test and evaluate the efficiency and stability of the aforementioned algorithm. Three different scenarios for a six-layer model can be considered: Model A (increasing wave speed with depth), Model B (a soft layer trapped between two hard layers, LVL), and Model C (a hard layer enclosed between two soft layers, HVL). Table 1 shows the velocity characteristics of all three hypothetical six-layer models. The frequency range for all three cases was set between 0.5-30 Hz, with a sampling interval 50. In this study, the simultaneous inversion of longitudinal wave speed, shear wave speed, and thickness were performed under the assumption of a Poisson's ratio (0.2 < Poisson's ratio < 0.5). The initial search space was also set to ±50% of the assumed model values. Fig.s 3 to 5 illustrate the inversion of the fundamental mode of Rayleigh waves for Models A, B, and C. In all models, after 50 iterations, the convergence of the misfit function reached its minimum possible value, and increasing the number of iterations did not enhance convergence further. In all Fig.s, the actual model is compared with the model obtained from the inversion of the fundamental mode of Rayleigh waves. The standard deviation and relative error indicate a better match between the actual and estimated models in shallower layers than deeper ones. The highest error was observed in the inversion of the thickness parameters for the fourth and fifth layers. Overall, the calculated error values for speed parameters are less than those for thickness parameters. The results for Model B (LVL) demonstrate the high accuracy of the method in modeling low-speed layer parameters. Boundary failure methods are generally unable to determine low-speed layers; in such cases, using surface wave inversion will udoubtedly be effective. The same conclusion applies to Model C (HVL). In summary, based on the conducted evaluations, the algorithm's efficiency for solving the surface wave inversion problem is confirmed.

B. Initial Model Generation and Evaluation Criteria in Ant Colony Optimization (ACO)

In the ACO-based inversion approach, the initial model is generated randomly within predefined parameter bounds. These bounds are determined based on prior geological knowledge, borehole data, and empirical relationships. The primary parameters include shear wave velocity (V_S), compressional wave velocity (V_p), and layer thickness. Each artificial ant constructs a candidate solution (V_S profile) by sampling from these parameter ranges. The initial pheromone distribution is set uniformly, ensuring an equal probability of selecting different paths at the start of the optimization process.

The evaluation of the model's performance is conducted using a fitness function that quantifies the misfit between the experimental and synthetic dispersion curves. The objective function, often defined as the root mean square error (RMSE) or least-squares misfit, minimizes the difference between observed and modeled phase velocities. Convergence is achieved when the reduction in misfit reaches a predefined threshold, or when additional iterations fail to yield significant improvements.

C. Potential Limitations and Challenges of ACO for Dispersion Curve Inversion

While ACO has proven effective for nonlinear optimization, it has some inherent challenges:

- **Computational Cost:** ACO requires multiple iterations with many ants to ensure global exploration, leading to high computational demands.
- **Parameter Sensitivity:** The choice of parameters such as pheromone evaporation rate (ρ) and heuristic weighting coefficients (α, β) can significantly impact convergence speed and solution accuracy.
- **Local Minima Avoidance:** Although ACO mitigates local minima issues better than traditional gradient-based methods, improper tuning of algorithmic parameters may still lead to suboptimal solutions.
- **Initial Model Dependence:** While ACO does not require a predefined deterministic model, the quality of initial parameter bounds can influence inversion outcomes, potentially biasing the search space.
- **Scalability:** The algorithm's performance may degrade when applied to highly heterogeneous or deep geological structures due to the increased complexity of the parameter space.

Despite these limitations, ACO remains a robust tool for dispersion curve inversion, offering flexibility in exploring complex subsurface structures while maintaining a balance between exploration and exploitation.

D. Comparison of Ant Colony Optimization Algorithm with Neighborhood Algorithm Used in Geopsy Software

Model A was utilized to compare the Ant Colony Optimization (ACO) algorithm with the neighborhood algorithm implemented in Geopsy software. Both algorithms were tested with identical search spaces (±50% of assumed model values) and a fixed number of 50 iterations. To quantify their performance, we evaluated accuracy, convergence rate, and computational efficiency. Fig. 6 presents the inversion results using the neighborhood algorithm, showing a reasonable fit between the actual and modeled dispersion curves but a poorer match for the shear wave speed (V_S) profile. In contrast, ACO achieved a closer alignment with the true V_S profile. Quantitatively, ACO yielded a misfit of 3×10^{-4} with a mean relative error of 3.5% for speed parameters, while the neighborhood algorithm produced a misfit of 8×10^{-3} and a mean relative error of 15%. Furthermore, ACO converged to its minimum misfit within 50 iterations, requiring an average runtime of 12.5 minutes on a standard workstation (Intel Core i7, 16 GB RAM), compared to 15.2 minutes for the neighborhood algorithm under the same conditions. This demonstrates ACO's superior accuracy and computational efficiency. However, ACO's performance depends on carefully tuning parameters such as the pheromone evaporation rate (ρ = 0.1 in this study) and the number of ants (50), which we optimized through preliminary trials to balance exploration and convergence.

This comparison reveals the capabilities of both algorithms in terms of inverting Rayleigh wave dispersion curves obtained from complex models. However, the accuracy and efficiency of the algorithm presented in this study appear to be superior.

E. Inversion of Experimental Data

In this section, experimental dispersion curves, acquired from a station in the central plain of the city, replace synthetic data for algorithm evaluation. Initial parameterization values are outlined in Table 2. Based on the dispersion curve morphology, a four-layer model—comprising three alluvial layers overlying bedrock—was selected for inversion. Due to limited subsurface geological data, a broad range of thicknesses was considered for each layer. Similarly, wide ranges of shear wave velocity (V_S) and longitudinal wave velocity (V_p) were incorporated. Both V_p and V_S parameters were included in the inversion process, while layer density was held constant. Following the inversion of the Rayleigh wave dispersion curve, a robust quantitative and qualitative interpretation of the soil layering was achieved. To validate the results, the inverted model was compared with data from nearby boreholes. Fig. 7 presents the inversion outcomes for the experimental

data. Consistent with its efficacy in modeling synthetic dispersion curves, the Ant Colony Optimization (ACO) algorithm exhibited strong performance in inverting experimental curves. Fig. 7(a) displays a photograph of a drilled borehole near the sampling site. Fig. 7(b) illustrates the shear wave velocity profile, with blue lines representing the inverted V_S profile and its standard deviation, bounded by green dashed lines indicating the upper and lower search limits. Fig. 7(c) compares the experimental dispersion curve (blue points, including standard deviation bounds) with the modeled curve (red line), revealing an excellent match. Fig. 7(d) depicts the misfit function's evolution across iterations, reaching a value of 4×10^{-4} after 50 iterations, further confirming the high agreement between experimental and modeled curves. Comparison with borehole data reveals strong correspondence in layering and an increasing trend in V_S with depth.

IV. Two-Dimensional Shear Wave Speed Model of Tabriz Plain

In this stage, based on geophysical studies (microtremor arrays), shear wave speeds were initially obtained in a one-dimensional format in Tabriz and, subsequently, presented as two-dimensional geological profiles (by integrating the geophysical results, existing boreholes, and geological maps of Tabriz). Regarding calibrating data with collected data, it is important to note the following:

-The drilling logs from the regional water company had very low accuracy due to appropriate depth, and no geophysical data were available within these boreholes as most were outside the area.

-The geoelectric studies conducted were also outside the urban area and were not usable.

-The drilling logs from the municipality had reasonable accuracy but were very shallow, hence being incompatible with the goals of the present study.

-A few logs from the Housing and Urban Development Organization and downhole seismic data performed in them were also unreliable due to shallow depth and the very low accuracy of shear wave measurements (only longitudinal waves had adequate accuracy).

-The only credible reference was the 1:25,000 geological map of Tabriz 1 and 2, which was going to be used for this study; however, unfortunately, as of the time of writing this report, the maps have not been approved and are not publishable.

In conclusion, it should be noted that the aim of this study is solely to estimate shear wave speeds in soil, not to characterize soil layering based on regional lithology. In Fig. 8, the extracted profiles are located on the 1:100,000 geological map of Tabriz, followed by the shown two-dimensional modeled profiles.

A. Statistical Evaluation of Model Accuracy

To assess the accuracy of the estimated shear wave velocity (V_S) profiles, we compare the inversion results against independent borehole and geophysical measurements using the following statistical metrics:

- Root Mean Square Error (RMSE):

This metric quantifies the average deviation between the inverted and observed velocity values, with lower RMSE values indicating better model fit.

$$RMSE = \sqrt{\frac{1}{n}\sum_{i=1}^{n}\left(V_{S_{\text{inverted}}} - V_{S_{\text{observed}}}\right)^2} \quad (7)$$

- Mean Absolute Percentage Error (MAPE):

MAPE provides a percentage-based error measure, making it helpful in assessing relative accuracy across different depths.

$$MAPE = \frac{1}{n}\sum_{i=1}^{n}\left|\frac{V_{S_{\text{inverted}}} - V_{S_{\text{observed}}}}{V_{S_{\text{observed}}}}\right| * 100 \quad (8)$$

- Pearson Correlation Coefficient (R^2):

This metric evaluates the strength of the relationship between the estimated and observed values, with values closer to 1 indicating a stronger correlation.

$$R = 1 - \frac{\sum_{i=1}^{n}\left(V_{S_{\text{inverted}}} - V_{S_{\text{observed}}}\right)}{\sum_{i=1}^{n}\left(V_{S_{\text{observed}}} - \bar{\ }\right)} \quad (9)$$

In these Eq.s, $V_{S_{\text{inverted}}}$ represents the predicted values (or simulated values$V_{S_{\text{observed}}}$represents the observed values and n is the number of observations.

V. Case Studies and Practical Implementations

Several previous studies have demonstrated the effectiveness of metaheuristic optimization techniques, including Ant Colony Optimization (ACO), in geophysical applications. Below are key case studies that illustrate the practical significance of our approach:

- **Shear Wave Velocity Profiling in Urban Areas**
  Cercato (2009) and Foti et al. (2009) applied inversion techniques to map subsurface shear wave velocity in densely populated urban settings. Their work demonstrated that metaheuristic algorithms significantly improve the resolution of velocity models, aiding seismic hazard assessment.
- **Basin Structure Characterization Using Surface Waves**
  Maghami et al. (2021) used microtremor inversion combined with metaheuristic algorithms to extract shear wave velocity structures of deep alluvial basins in Iran. Their findings confirmed that such methods provide

robust, high-resolution, subsurface models that align well with borehole data.

- **Seismic Site Response Studies**
  Angardi et al. (2024) integrated artificial intelligence-driven inversion techniques with experimental data to estimate Rayleigh wave ellipticity curves, enhancing the accuracy of Vs profiling. The results were validated against geotechnical site investigations.

These case studies highlight the growing acceptance and success of metaheuristic approaches in geophysical studies. Our work builds upon these advancements by further refining ACO for dispersion curve inversion, demonstrating its ability to provide accurate and computationally efficient solutions in complex geological environments. Fig. 9 shows the research process in this article.

VI. Conclusions

The main objective of the present study is to present a new algorithm aimed at improving the inversion of surface wave dispersion curves to obtain the shear wave velocity structure of the ground. Collective intelligence algorithms such as ant colony optimization function well in solving nonlinear problems with multiple extrema. Their low sensitivity to local minima or maxima enhances their appeal. Like other global search methods, these approaches do not require an initial model and explore the entire parameter space defined beforehand for solving the problem. Therefore, there is no risk of getting trapped in local minima or maxima. In these algorithms, many layers and a wide range of velocity and thickness values are selected. The general trend, where velocity increases or decreases with depth, can be determined based on the shape of the dispersion curve and using the empirical rule $\lambda/2$. Running the algorithms multiple times to obtain the final model is effectively improves results, allowing for the definition of the average model and standard deviation for each model parameter. To test the efficiency of the introduced algorithms, the inversion of dispersion curves obtained from three cases of a six-layer model was used. Since the longitudinal wave velocity has a very minor (and non-negligible) effect compared to the shear wave velocity in surface wave dispersion curves, simultaneous inversion of both parameters (0.1 < Poisson's ratio < 0.5) was performed to enhance results. Unlike fracture seismic methods, using surface wave inversion performs well in differentiating low-velocity layers. The error in calculating the shear wave velocity for all layers is low; however, the relative error for thickness parameters, especially in intermediate layers, is significant. Overall, using ant colony optimization algorithms indicates successful inversion of artificial surface wave dispersion curves. Additionally, the present study employed ant colony optimization alongside a neighborhood algorithm. A comparison between the proposed algorithm and the neighborhood algorithm used in the software (Geopsy) shows greater convergence and accuracy of the ant colony optimization algorithm. Two-dimensional modeling generally indicates that shear wave velocity in Tabriz increases rapidly with depth, while the velocity values are moderate in surface layers, except for the weathered layer. Furthermore, studying shear wave velocity profiles reveals that in the northern and southern parts, shear wave velocity is higher, indicating an uplift of the bedrock.

Refrerences

Aki, K., 1957- Space and time spectra of stationary stochastic waves, with special reference to microtremors: Bulletin of the Earthquake Research Institute, v.35, p.415-456.

Ali, M. S., Saeed, K., Jianxun, M., Dong, L., & Ali, L. (2024). Deep soil seismic hazard assessment: analyzing the impact of local site effects by stochastic site response analysis—a comparative approach. Bulletin of Engineering Geology and the Environment, 83(6), 1-31.

Angardi, S., Poursorkhabi, R. V., Shirvanehdeh, A. Z., & Dabiri, R. (2024). Vs Profiling by the Inversion of Rayleigh Wave Ellipticity Curve Using a Hybrid Artificial Intelligence Method. Pure and Applied Geophysics, 1-14.

Beaty, K. S., Schmitt, D. R. & Sacchi, M., 2002- Simulated annealing inversion of multimode Rayleigh wave dispersion curves for geological structure: Geophysical Journal International, v.151, p.622-631.

Beheshtifar, K., & Poursorkhabi, R. V. (2024). Experimentally calibrated finite element fatigue reliability assessment of an offshore platform in the Persian Gulf. Journal of Ocean Engineering and Marine Energy, 1-11. https://doi.org/10.1007/s40722-023-00311-z

Boore, D., 2006- Determining subsurface shear-wave velocities: a review. Presented at the Third International Symposium on the effects of surface geology on seismic motion, Grenoble, France, 103.

Cercato, M., 2009. Addressing non-uniqueness in linearized multichannel surface wave inversion: Geophysical Prospecting, v.57, p.27-47. https://doi.org/10.1111/j.1365-2478.2007. 00719.x

Cruz, L., Todorovska, M. I., Chen, M., Trifunac, M. D., Aihemaiti, A., Lin, G., & Cui, J. (2024). For how large soil shear wave velocity the soil-structure interaction effects on a tall building can be neglected–A case study. Soil Dynamics and Earthquake Engineering, 184, 108845. https://doi.org/10.1016/j.soildyn.2024.108845

Dal Moro, G., Pipan, G. & Gabrielli, M. P., 2007- Rayleigh wave dispersion curve inversion via genetic algorithms and marginal posterior probability density estimation: Journal of Applied Geophysics, v.61(1), p.39-55.
https://doi.org/10.1016/j.jappgeo.2006.04.002

Dorigo, M., V. Maniezzo, and A. Colorni, 1996. The Ant system: Optimization by a colony of cooperating agents. IEEE Trans. Syst. Man Cybernet, Part B, 26, 29-41. https://doi.org/10.1109/3477.484436

Duan, H. & Yu, X., 2007- Progresses and Challenges of Ant Colony Optimization based Evolvable Hardware: Proceedings of the 2007 IEEE Workshop on Evolvable and Adaptive Hardware (WEAH), p.67-71.
https://doi.org/10.1109/WEAH.2007.361715

Farrugia, D., Paolucci, E., D'Amico, S., & Galea, P. (2016). Inversion of surface wave data for subsurface shear wave velocity profiles characterized by a thick buried low-velocity layer. Geophysical Journal International, 206(2), 1221-1231.

Foti, S., Comina, C., Boiero, D. & Socco, L. V., 2009- Non-uniqueness in surface wave inversion and consequences on seismic site response analyses: Soil Dynamics and Earthquake Engineering, v.29, p.982-993. https://doi.org/10.1016/j.soildyn.2008.11.004

Haskell, N.A., 1953- The dispersion of surface waves on a multi-layered medium: Bulletin of the Seismological Society of America, v.43, p.17-34. https://doi.org/10.1029/SP030p0086

Herrmann, R. B. & Ammon, C. J., 2004- Surface wave inversion: Computer program in seismology, Ver. 3.3, Saint Louis University.

Hunter, J., Benjumea, B., Harris, J., Miller, R., Pullan, S. & Burns, R. A., 2002- Surface and down hole shear wave seismic methods for thick soil site investigations: Soil Dynamics and Earthquake Engineering, v.22(9-12), p.931-941. https://doi.org/10.1016/S0267-7261(02)00117-3

Jongmans, D., 1992- The application of seismic methods for dynamic characterization of soils in earthquake engineering: Engineering Geology, v.46(1), p.63-69. https://doi.org/10.1007/BF02595035

Li, T., Chen, W., Zheng, X. & Zhang, Z., 2009- An Improvement of The Ant Colony Optimization Algorithm for Solving Travelling Salesman Problem (TSP): IEEE Cnference Proceedings, 2009. https://doi.org/10.1109/WICOM.2009.5302937

Luo, Y., Xia, J., Miller, R. D., Xu, Y., Liu, J. & Liu, Q., 2009- Rayleigh-wave mode separation by high-resolution linear Radon transform: Geophysical Journal International, v.179(1), p.254-264. https://doi.org/10.1111/j.1365-246X.2009.04277.x

Maghami, s., Sohrabi-Bidar, A., Bignardi, S., Zarean, A., Kamalian, M., (2021) Extracting the shear wave velocity structure of deep alluviums of "Qom" Basin (Iran) employing HVSR inversion of microtremor recordings, Journal of Applied Geophysics 185, 104246. https://doi.org/10.1016/j.jappgeo.2020.104246

Maleki, M. Kh ., Poursorkhabi, R. V., Nadiri, AA. & Dabiri, R., 2022- Prediction of hydraulic conductivity based on the soil grain size using supervised committee machine artificial intelligence, 15 (4), 2571-2583. https://doi.org/10.1007/s12145-022-00848-x

McMechan, G.A. & Yedlin, M.J., 1981- Analysis of dispersive waves by wave field transformation: Geophysics, v.46, p.869-874. https://doi.org/10.1190/1.1441225

Nemati, Sh. & Basiri, M.E., 2011- Text-independent speaker verification using ant colony optimization-based selected features: Expert Systems with Applications, v.38, p.620-630. https://doi.org/10.1016/j.eswa.2010.07.011

Poormirzaee, R., (2016) S-wave velocity profiling from refraction microtremor Rayleigh wave dispersion curves via PSO inversion algorithm, Arab J Geosci 9:1-10. https://doi.org/ 10.1007/s12517-016-2701-6

Pouraziz, H., Vafaei Fard, M. Y., & Dabiri, R. (2024). Effects of wollastonite powder on the geotechnical properties of a dispersive clayey soil. Discover Applied Sciences, 6(8), 433. https://doi.org/ 10.1007/s42452-024-06133-4

Poursorkhabi, R. V., & Ghasempour, R. (2019). Possibilities to use the meta model and classical approaches to evaluate the impact of hydraulic conditions in prediction of the critical submergence depth ratio. Water Supply, 19(4), 1055-1065. https://doi.org/10.2166/ws.2018.153

Renalear, F., Jongmans, D., Savvaidis, A., Wathelet, M., Endrun, B. & Cornou C. 2010- Influence of parameterization on inversion of surface wave dispersion curves and definition of an inversion strategy for sites with a strong VS contrast: Geophysics, v.75(6), p.197-209. https://doi.org/10.1190/1.3506556

Roberts, J.C. & Asten, M.W., 2004- Resolving a velocity inversion at the geotechnical scale using the microtremor (passive seismic) survey method: Exploration Geophysics, v.35, p.14-18. https://doi.org/10.1071/ASEG2004ab122

Rui, X., Zhang, J., Wang, X., Rong, B., He, B., & Jin, Z. (2022). Multibody system transfer matrix method: the past, the present, and the future. International Journal of Mechanical System Dynamics, 2(1), 3-26. https://doi.org/10.1002/msd2.12037

Socco, L.V. & Boiero, D., 2008- Improved Monte Carlo inversion of surface wave data: Geophysical Prospecting, v.56, p.357-371. https://doi.org/10.1111/j.1365-2478.2007.00678.x

Socco, L.V., Foti, S. & Boiero, D., 2010- Surface-wave analysis for building near-surface velocity models-Established approaches and new perspectives. Geophysics, v.75(4), p.83-102. https://doi.org/10.1190/1.3479491

Somerville, P.G. & Graves, R. W., 2003- Characterization of earthquake strong ground motion: Pure and Applied Geophysics, v.160(10-11), p.1811-1828. https://doi.org/10.1007/s00024-003-2407-z

Tian, Z., Xiao, W., Ma, Z., & Yu, L. (2021). Dispersion curve regression–assisted wideband local wavenumber analysis for characterizing three-dimensional (3D) profile of hidden corrosion damage. Mechanical Systems and Signal Processing, 150, 107347. https://doi.org/10.1016/j.ymssp.2020.107347

Wathelet, M., Jongmans, D. & Ohrnberger, M., 2004- Surface wave inversion using a direct search algorithm and its application to ambient vibration measurements: Near Surface Geophysics, v.2, p.211-221. https://doi.org/10.3997/1873-0604.2004018

Yamanaka, H. & Ishida, H., 1996- Application of genetic algorithms to an inversion of surface-wave dispersion data: Bulletin of the Seismological Society of America, v.86, p.436-444. https://doi.org/10.1785/BSSA0860020436

Yilmaz, Ö., 1987- Seismic data processing: Society of Exploration Geophysicists, Tulsa, OK.

Zarean A, Mirzaei N, Mirzaei M (2015) Applying MPSO for Building Shear Wave Velocity Models from microtremor wave Dispersion Curves. J. Seism. Explor. 24, 1–20.

Zareh, A., Poursorkhabi, R. V., Majdi, A. A., & Sarand, F. B. (2023). The efficiency of the electro-osmosis method on the consolidation and strength properties of the gray clay of Tabriz. Geoenvironmental Disasters, 10(1), 16. https://doi.org/10.1186/s40677-023-00245-6.

Table 1. The reference model of six layers (A, B, And C) to evaluate the efficiency and stability of the ant colony algorithm

	Layer	Thickness (m)	50% Search Space	*Vp* (m/s)	50% Search Space	*Vs* (m/s)	50% Search Space	Density (kg/m³)
Model A	1	20	10-30	600	300-900	200	100-300	1800
	2	10	5-15	900	450-1350	300	150-450	1900
	3	30	15-45	1200	600-1800	400	200-600	1900
	4	40	20-60	1500	750-2250	500	250-750	2000
	5	50	25-75	2100	1050-3150	700	350-1050	2000
	6	Half-space	------	3000	1500-4500	1000	500-1500	2100
Model B	1	10	5-15	600	300-900	200	100-300	1800
	2	20	10-30	450	225-675	150	75-225	1900
	3	30	15-45	900	450-1350	300	150-450	1900
	4	40	20-60	1200	600-1800	400	200-600	2000
	5	50	25-75	1800	900-2700	600	300-900	2000
	6	Half-space	------	3000	1500-4500	1000	500-1500	2100
Model C	1	10	5-15	450	225-675	150	75-225	1800
	2	20	10-30	750	375-1125	250	125-375	1900
	3	30	15-45	600	300-900	200	100-300	1900
	4	40	20-60	1200	600-1800	400	200-600	2000
	5	50	25-75	1800	900-2700	600	300-900	2000
	6	Half-space	------	3000	1500-4500	1000	500-1500	2100

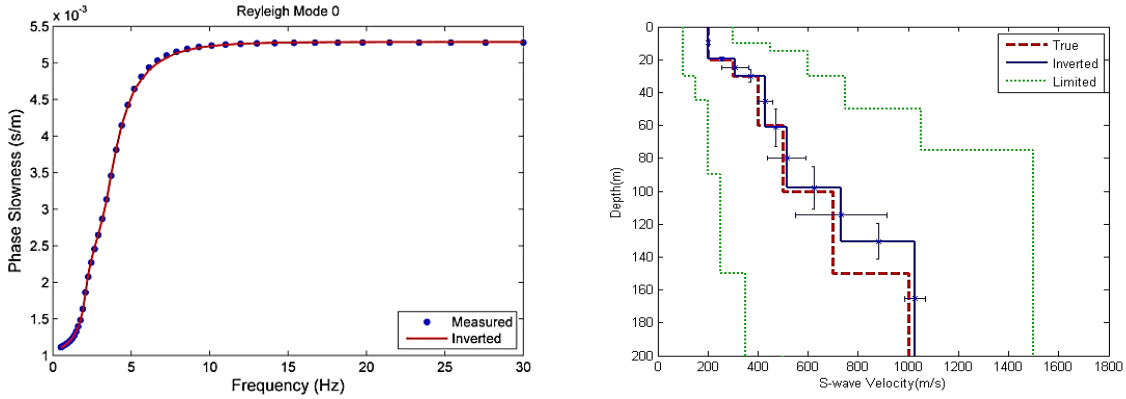

(*a*) (*b*)

Fig. 3. Inverted spray curve of model A using the Ant Colony Optimization algorithm. (*a*) Base modal data of Rayleigh wave (blue dots) and the modeled spray curve (red line), (*b*) Lower and upper limits of the search range (50%) (green dashed line), actual model (red dashed line), and shear wave velocity profile along with standard deviation values (solid blue line).

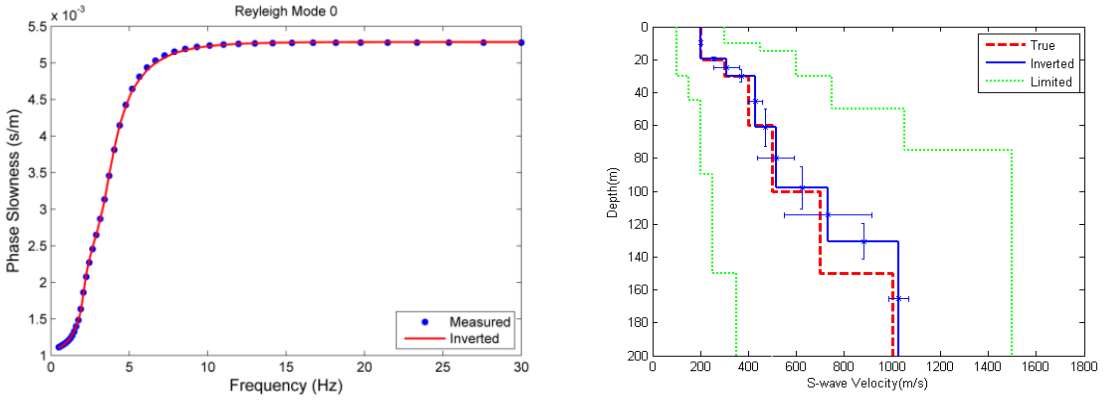

(*a*) (*b*)

Fig. 4. Inverted spray curve of model B using the Ant Colony Optimization algorithm. (*a*) Base modal data of Rayleigh wave (blue dots) and the modeled spray curve (red line), (*b*) Lower and upper limits of the search range (50%) (green dashed line), actual model (red dashed line), and shear wave velocity profile along with standard deviation values (solid blue line).

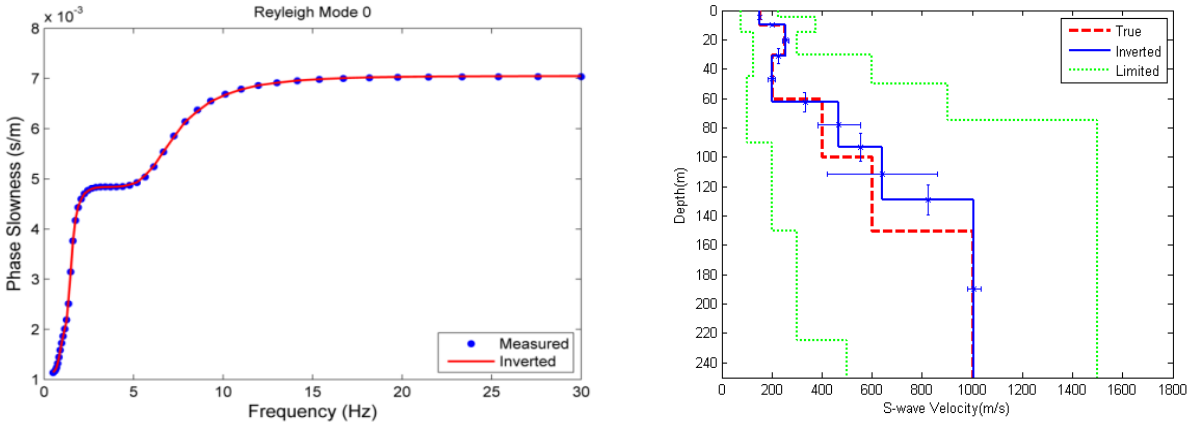

(*a*) (*b*)

Fig. 5. (*a*) Inverted spray curve of model C using the Rayleigh wave (blue points) and the modeled spray curve (red line), (*b*) Lower and upper limits of the search range (50%) (green dashed line), actual model (red dashed line), and shear wave velocity profile along with standard deviation values (blue solid line).

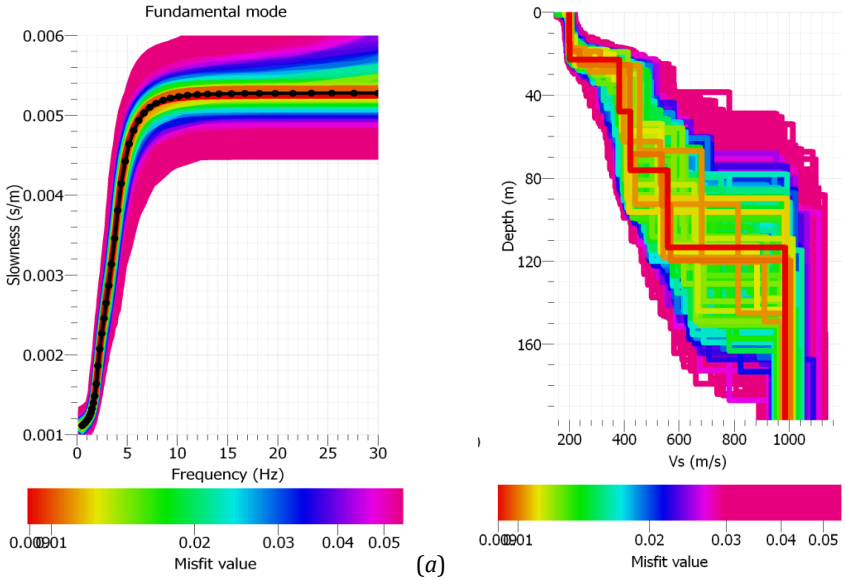

(*a*) (*b*)

Fig. 6. Inverted spray curve of model A using the neighborhood algorithm. (*a*) Base mode data of Rayleigh wave (black points) and the modeled spray curve along with the misfit function values (colored lines), (*b*) Actual model (black dashed line), shear wave velocity profile along with the misfit function values (colored lines)

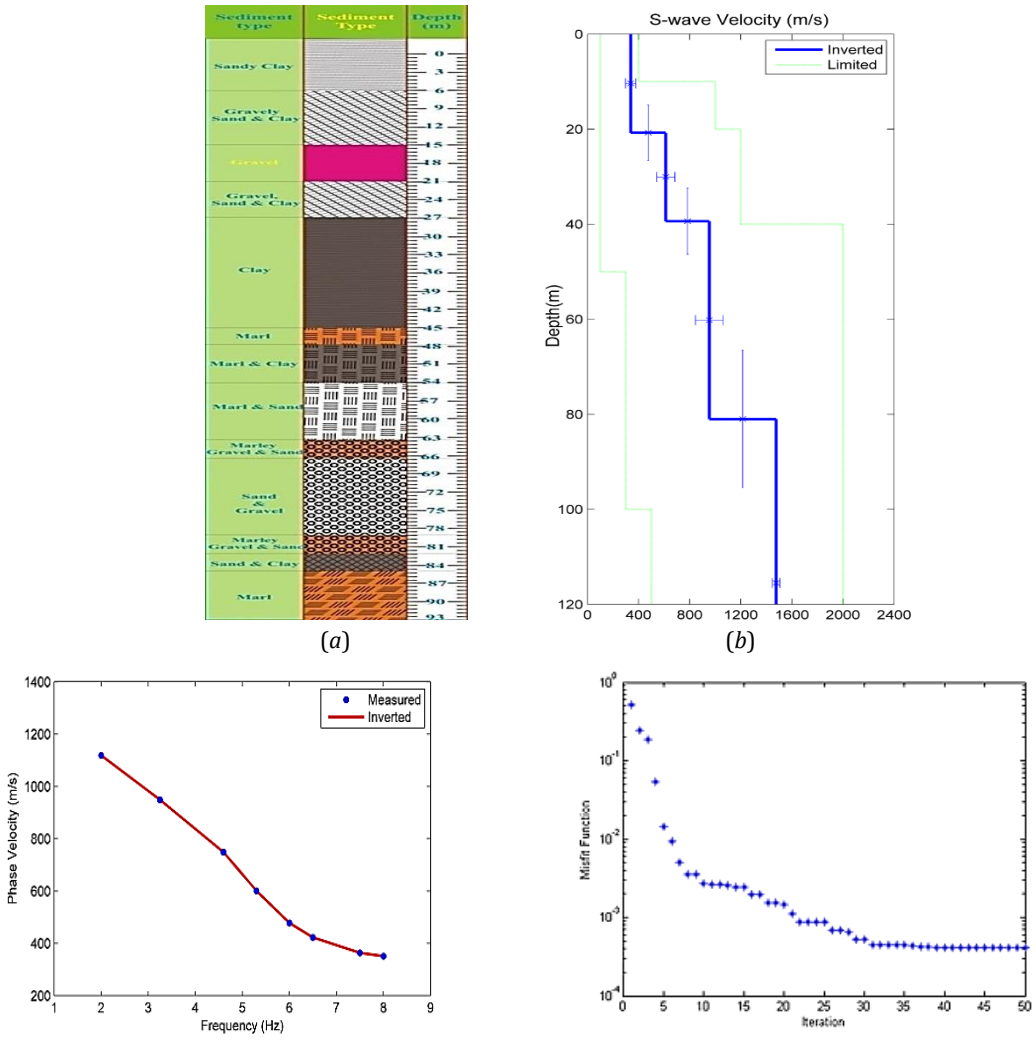

(*a*) (*b*)

(*c*) (*d*)

Fig. 7. Experimental data inversion, (*a*) Borehole log, (*b*) Shear wave velocity profile (blue line) and search space (green dotted line), (*c*) experimental spray curve (blue dots) and modeled spray curve (red line), (*d*) changes of misfit function against repetition

Table 2. How to parameterize the experimental spray curve to evaluate the Aco Algorithm

	Layer	Thickness (m) Search Space	V_P (m/s) Search Space	V_S (m/s) Search Space	Density (kg/m³)
Field Data	1	10-50	400-1200	100-400	1800
	2	10-50	800-2000	300-1000	2000
	3	20-60	1000-3000	500-1200	2000
	4	Half-space	2000-4000	800-2000	2100

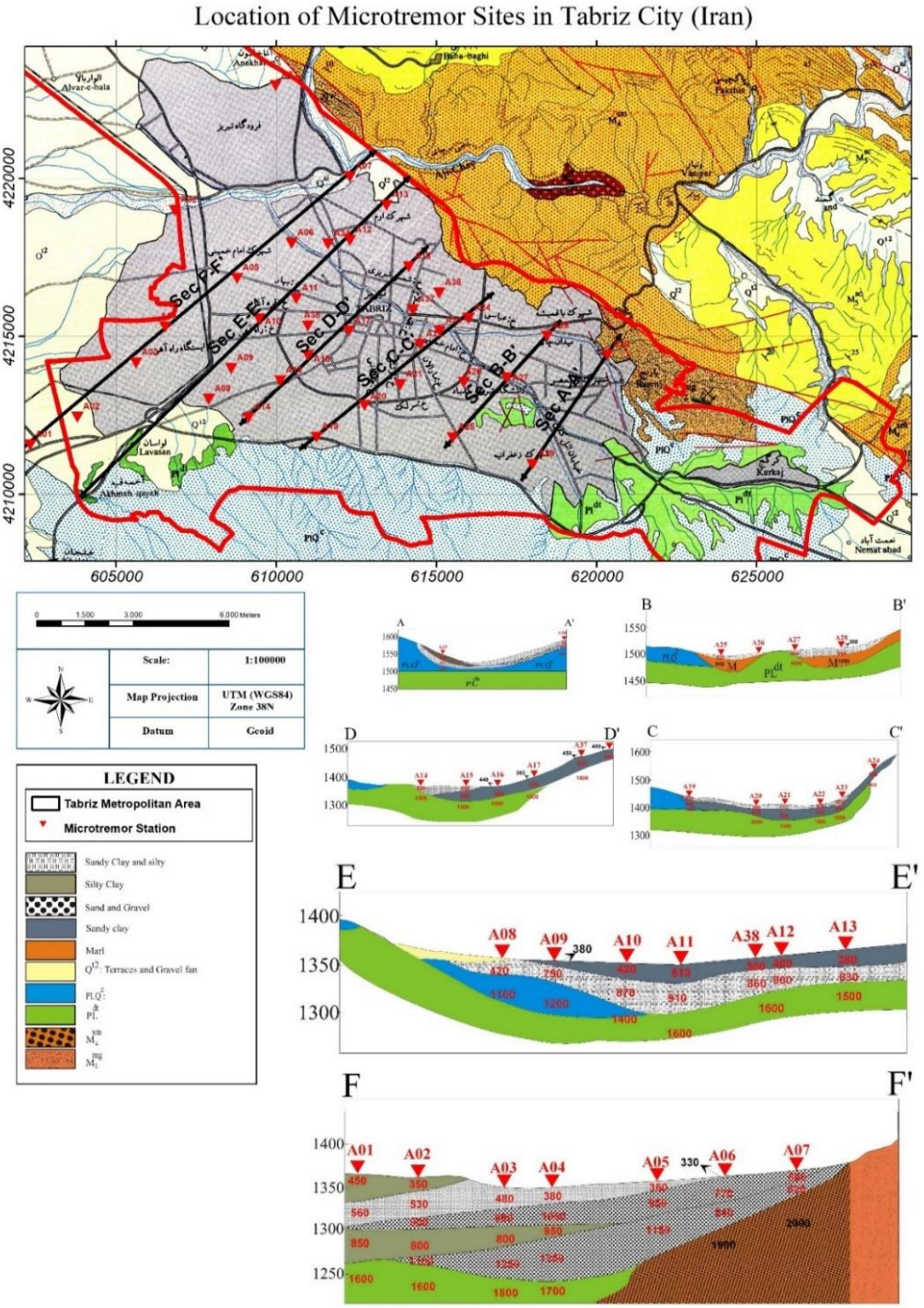

Fig. 8. Location of the measurement points of microtremor arrays and the modeled Vs profiles on the geological map of Tabriz at a scale of 1:100,000 (shear wave velocity units in the profiles are in m/s).

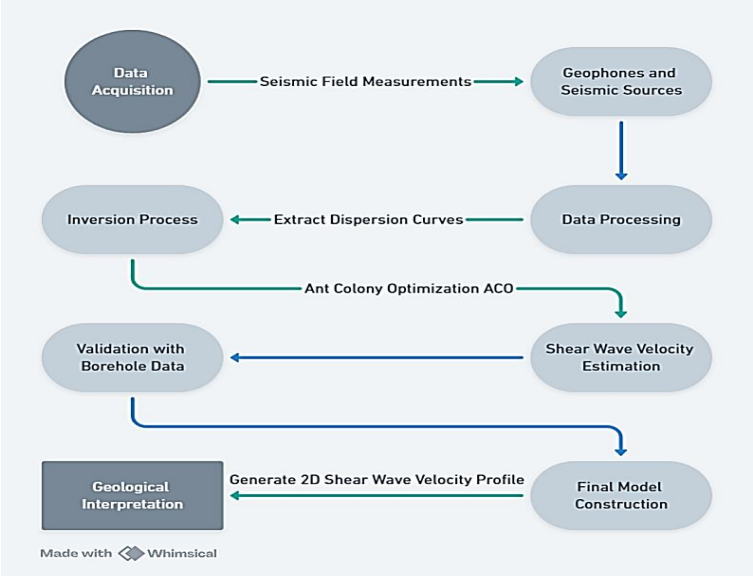

Fig. 9. Workflow of methodology